Journal of Physiology - Paris 102 (2008) 181–194

Contents lists available at ScienceDirect

Journal of Physiology - Paris

journal homepage: www.elsevier.com/locate/jphysparis

Regulation of somatic firing dynamics by backpropagating dendritic spikes

W. Hamish Mehaffey [a], Fernando R. Fernandez [a,1], Brent Doiron [b,2], Ray W. Turner [a,*]

[a] Hotchkiss Brain Institute, University of Calgary, 3330 Hospital Dr. N.W., Calgary, Alberta, Canada T2N 4N1
[b] Center for Neural Science and Courant Institute of Mathematical Sciences, New York University, New York, NY 10012, USA

ARTICLE INFO

Keywords:
Burst dynamics
Sensory processing
Electric fish
Synaptic integration
Backpropagation

ABSTRACT

Pyramidal cells of the apteronotid ELL have been shown to display a characteristic mechanism of burst discharge, which has been shown to play an important role in sensory coding. This form of bursting depends on a reciprocal dendro-somatic interaction, in which discharge of a somatic spike causes a dendritic spike, which in turn contributes a dendro-somatic current flow to create a depolarizing afterpotential (DAP) in the soma. We review here our recent work showing how the timing of this DAP influences the somatic firing dynamics, and how the degree of inactivation of dendritic Na^+ currents can cause an increased delay between somatic and dendritic spikes. This ultimately allows the DAP to become more effective at increasing the excitability of the somatic spike generating mechanism. Further, this delay between dendritic and somatic spiking can be regulated by strongly hyperpolarizing $GABA_B$ mediated dendritic inhibition, allowing the burst dynamics to fall under synaptic regulation. In contrast, a weaker, shunting inhibition due to $GABA_A$ mediated dendritic inhibition can regulate the dendritic spike waveform to decrease the dendro-somatic current flow and the resulting DAP. We therefore show that the qualitative behaviour of an individual cell can depend on the degree of synaptic input, and the exact timing of events across the spatial extent of the neuron. Thus, our results serve to illustrate the complex dynamics that can be observed in cells with significant dendritic arborisation, a nearly ubiquitous adaptation amongst principal neurons.

1. Introduction

Single spikes have been widely assumed to be the primary mediator of neuronal coding (Rieke, 1997), but there has been a recent explosion of interest in clusters of spikes, often termed bursts, as important elements of the neural code (Eggermont and Smith, 1996; Gabbiani et al., 1996; Krahe and Gabbiani, 2004; Lesica and Stanley, 2004; Lesica et al., 2006; Lisman, 1997; Oswald et al., 2004; Wang et al., 2006). One particular system where bursting has been well characterized in vitro (Lemon and Turner, 2000; Turner et al., 1994), in vivo (Gabbiani et al., 1996; Metzner et al., 1998; Oswald et al., 2004), in models (Doiron et al., 2002, 2001a,b; Laing and Longtin, 2002; Laing et al., 2003; Fernandez et al., 2005b), and within the context of sensory coding has been in the electrosensory lateral line lobe (ELL) of gymnotiform fish (*Apteronotus leptorhynchus*).

A. leptorhynchus is a wave-type weakly electric fish which generates a continuous electric organ discharge (EOD) by means of a specialized electric organ. One ability conferred by this high-frequency quasi-sinusoidal EOD is the ability to act as a carrier wave, allowing the amplitude modulations (AMs) caused by perturbations to be detected by specialized electroreceptors on the skin. These, in turn, project to the ELL, the first order of processing in the central nervous system of *Apteronotus*. Thus, at this point in processing, electroreception represents a specific example of a more general problem whereby complex sensory stimuli must be parsed by the nervous system in order to generate a representation of components of the external world. Relevant electrosensory stimuli include prey and environmental signals as well as inter-fish beat frequencies and communication calls (e.g. 'chirps'). Importantly, natural electrosensory stimuli have a wide range of frequency components and a varying spatial extent. In particular, prey and environmental signals are spatially localized ('local'), containing much of their power at frequencies below 10 Hz. In contrast, more spatially extended stimuli, including beat frequencies (resulting from interference with conspecific EODs) and communication calls, can contain much of their power at higher frequencies (>30 Hz). Work in the ELL has determined that these differences in frequency content can be exploited by burst dynamics in order to selectively code distinct aspects of an input (Mehaffey et al., 2007; Oswald et al., 2004).

* Corresponding author. Tel.: +1 403 220 8452; fax: +1 403 210 8119.
E-mail address: rwturner@ucalgary.ca (R.W. Turner).
URL: http://www.acs.ucalgary.ca/~rwturner/ (R.W. Turner).
[1] Present Address: Department of Bioengineering, University of Utah, Salt Lake, UT 84112, United States.
[2] Present Address: Department of Mathematics, University of Pittsburgh, Pittsburgh, PA 15206, United States.

0928-4257/$ - see front matter © 2008 Elsevier Ltd. All rights reserved.
doi:10.1016/j.jphysparis.2008.10.011

Sequences of patterned isolated spikes have been assumed to be the main channel for information transfer between neurons (Eggermont, 1998; Rieke, 1997), although the role of bursts in signal coding is gaining prominence, particularly in the context of sensory systems (Krahe and Gabbiani, 2004). A segregation of spike trains into bursts and single spikes has been observed in electric fish (Gabbiani et al., 1996; Oswald et al., 2004) and in the mammalian visual (Lesica and Stanley, 2004; Lesica et al., 2006) and auditory systems (Eggermont and Smith, 1996). A striking example is found in invertebrates where bursts, but not isolated spikes, predict behaviour (Marsat and Pollack, 2006). Using pattern classifier methods bursts have been suggested to code for input slope (Kepecs et al., 2002) and to segregate different dynamic components of stimuli (Doiron et al., 2007; Kepecs and Lisman, 2003; Oswald et al., 2007). In sensory systems, bursts have been shown to be the preferred response for low-frequency events (Lesica and Stanley, 2004; Lesica et al., 2006), and specifically in the ELL for feature detection of low-frequency components of a stimulus (Doiron et al., 2007; Gabbiani et al., 1996; Metzner et al., 1998; Oswald et al., 2004, 2007). As such, burst coding appears to be an extremely common adaptation with clear benefits to information coding. When information is parceled into two distinct ranges of interspike intervals (ISIs) each with its own stimulus selectivity, the system can take advantage with an appropriate postsynaptic threshold for spiking, short term synaptic plasticity, or the intrinsic dynamics of downstream cells in order to separate and decode information. These concepts have been analyzed in more detail elsewhere – in particular that bursts tend to be more reliably timed, show superior feature detection properties, and may be able to more reliably activate downstream cells than single spikes (Gabbiani et al., 1996; Izhikevich et al., 2003; Kepecs and Lisman, 2003; Lisman, 1997; Metzner et al., 1998).

Understanding the role for burst discharge in sensory coding requires knowledge of the dynamics underlying burst discharge. We review here our recent results on the intrinsic burst mechanism of ELL pyramidal cells, as well as work examining the deterministic modulation of ELL pyramidal cell gain and the feedback regulation of burst coding, and provide evidence that bursting is a conserved feature of electrosensory processing across a range of species.

2. Materials and methods

2.1. Electrophysiology

Weakly electric Brown Ghost knife fish (*A. leptorhynchus*), Black Ghost knife fish (*Apteronotus albifrons*), and Glass knife fish (*Eigenmannia virescens*) were obtained from local importers and maintained at 26–28 °C in fresh water aquaria in accordance with protocols approved by the University of Calgary Animal Care Committee. All experiments were performed on *A. leptorhynchus* unless otherwise stated. All chemicals were obtained from SIGMA (St. Louis, MO) unless otherwise noted. In all cases recordings were obtained from separate pyramidal cell somata or apical dendrites in in vitro slices. Animals were anaesthetized in 0.05% phenoxy-ethanol, and ELL tissue slices of 300–400 μm thickness were prepared as previously described (Turner et al., 1994). For recordings with microelectrodes slices were maintained by constant perfusion of ACSF (1–2 ml/min), and superfusion of humidified 95% O_2, 5% CO_2 gas. ACSF contained (in mM): 124 NaCl, 3 KCl, 25 $NaHCO_3$, 1.0 $CaCl_2$, 1.5 $MgSO_4$ and 25 D-glucose, pH 7.4. Pharmacological agents were ejected locally from a pressure micropipette containing HEPES buffered ACSF (in mM): 148 NaCl, 3.25 KCl, 1.5 $CaCl_2$, 1.5 $MgCl_2$, 10 HEPES, and 25 D-glucose, pH 7.4. Focal ejections were performed to either somatic (pyramidal cell layer) or proximal dendritic (ventral molecular layer) regions. Previous studies have shown that the stratus tractum fibrosum (sTf), provides a reliable barrier against diffusion (Turner et al., 1994). Recordings were made from pyramidal cells in the largest two ELL segments receiving inputs from amplitude coding primary afferents (centromedial and centrolateral segments). Bursting pyramidal cells were identified by their progression from a tonic to a characteristic burst firing mode after sufficient depolarization (Lemon and Turner, 2000; Turner et al., 1994). Antidromic spikes were generated using square wave stimulation pulses delivered through isolation units (0.1 ms, 1–50 V; Digitimer SIU) to bipolar electrodes (twisted 62 μm nichrome wire) placed on pyramidal cell axons within the plexiform layer. Current-clamp microelectrode recordings were obtained from the dendrite or soma using an Axoclamp 2-A amplifier (Axon Instruments) at a sampling rate of 10–40 kHz. On-cell dendritic patch and voltage-clamp recordings were obtained using a Multiclamp 700 A (Axon Instruments) at a sampling rate of 5 kHz. Dendrites were identified by their location in the ELL molecular layer. The patch electrode solution consisted of (in mM): KCl (140), EGTA (5), HEPES (10) $MgCl_2$ (2.5). The membrane potential in these recordings was estimated from the reversal of the single potassium channel *I–V* relation. The reversal value was -69.3 ± 2.8 mV ($n = 4$). On-cell patches were stepped from 60 mV to −50 mV, which translated into a step depolarization from −129 mV to −19 mV when the cell membrane potential offset was taken into account. All recordings were done at 20–23 °C.

2.2. Data analysis and modeling

All electrophysiological data were analysed in Matlab R2006a (Mathworks, Natick, MA) or Clampfit (Axon Instruments, Oakland, CA). Spike threshold was obtained from the first derivative of the voltage waveform. Data was plotted in Origin (OriginLab, Northhampton MA). For calculations of coherence and bursting in response to time-varying inputs frozen random-amplitude modulated (RAM) noise, low-pass filtered to contain power from 0–60 Hz, was used as an intracellular stimulation protocol. Spike trains were partitioned into bursts and isolated spikes using an interspike interval histogram method and inter-spike interval (ISI) discrimination criterion of 8 ms, in agreement with previous work which established that these ISIs are associated with the conditional backpropagation of dendritic spikes that characterize bursting (Lemon and Turner, 2000; Turner et al., 1994). This is also consistent with previous studies examining in vitro time-varying inputs, as burst ISIs can be readily defined using this value given the consistency of burst output between cells in vitro (Mehaffey et al., 2008; Oswald et al., 2004) Bursts and isolated spike trains were digitized into binary trains (Bin Width, 0.5 ms) and their mean subtracted (Rieke, 1997). Coherence estimates between the digitized spike trains and the original RAM stimulus were calculated as:

$$C(f) = \frac{P_{sr}(f)^2}{P_{ss}(f)P_{rr}(f)}$$

where P_{ss} and P_{rr} denote the power spectrum of the stimulus and the response, and P_{sr} denotes the cross-spectrum between the stimulus and response (e.g., the spike train) and f is frequency measured in Hz. Unless otherwise mentioned, all statistics are *t*-tests with statistical significance set to $p > 0.05$.

Two models were used in the manuscripts reviewed here. A large multi compartmental model of a reconstructed ELL pyramidal cell fill (Doiron et al., 2001b; Mehaffey et al., 2005) used to analyze the gain effects of dendritic inhibition is mentioned only briefly here. For analysis of PRCs and bifurcation analyses, a reduced two-compartmental model was used consisting of an active dendritic and an active somatic compartment coupled through a resis-

tance (Fernandez et al., 2005b; Mehaffey et al., 2007). As the full description of all the model parameters for both models is beyond the scope of this review, we suggest that interested readers consult the original manuscripts for specific details.

3. Results

3.1. Dendritic spikes produce a somatic DAP that increases somatic excitability and drives bursting

Backpropagating spikes in ELL pyramidal cells increase somatic excitability by both decreasing the somatic ISI and driving the cell into burst firing (reviewed in (Turner et al., 2002)). This process can be considered as having two components – a fast component consisting of the spike generation mechanism, as well as a slow component consisting of the gradual increase in spike frequency and the resulting burst AHP (bAHP). The key element driving the slow component of this process is the frequency-dependent change in dendritic spike waveform. This change in waveform consists of an increase in spike duration and decrease in spike amplitude. We recently completed a study on the role of the depolarizing afterpotential (DAP) in modifying cell excitability, and on the biophysical basis for the frequency-dependent changes in dendritic properties that regulate the DAP and its influence on somatic firing dynamics (Fernandez et al., 2005b). The change in somatic excitability attributable to dendritic Na^+ current was established by focally ejecting tetrodotoxin (TTX) in the dendrites and measuring somatic ISI. This procedure is readily applied in the ELL, where diffusion of TTX to the somatic region is hampered by a thick axon tract that separates the pyramidal cell layer and the molecular layer where dendrites project (as established previously in Turner et al., 1994). Such techniques can also be applied effectively even in regions lacking such an anatomically convenient tract (Turner et al., 1991). In order to ensure that TTX did not block somatic Na^+ channels we also monitored somatic spike height. Under control conditions, depolarizations (0.25–0.7 nA) evoked somatic spikes whose ISI decreased with each successive spike in a burst (Fig. 1A). The ISI ranged from 7.8–5.5 ms for the first two spikes and 4.4–3.1 ms for the last two spikes in a burst train. Focal pressure application of TTX at the dendrites was able to eliminate the progressive decrease in somatic ISI (Fig. 1B), with ISI values ranging from 9.5–6.4 ms for the first two spikes but then remaining nearly constant throughout the spike train. These experiments show that dendritic Na^+ currents act as the primary source of an increase in somatic excitability leading to burst output (Fernandez et al., 2005b; Lemon and Turner, 2000; Turner et al., 1994).

3.2. The DAP has an inherently multiplicative effect on gain

Gain is a quantitative measure of the responsiveness of the cell to a given input, measured in Hz/nA. This defines the degree of change in the spike rate in response to a change in the input current, and is often taken to be the slope of the frequency–current (FI) curve. We examined the contribution of the dendritic spike to patterns of somatic output by blocking active dendritic spike propagation through focal application of TTX to the proximal dendritic region, as performed above. The immediate effect of dendritic TTX application on somatic membrane potential was to selectively remove the DAP, revealing a large somatic after hyperpolarization (AHP) which had been previously masked by the active dendritic conductances (Fig. 1C). No significant decrease in the peak amplitude or rate of rise of the somatic spike was observed, confirming that these actions were not due to TTX diffusing to the somatic region. Coincident with a block of the DAP, the FI curve showed a marked reduction in gain (Fig. 1D). The unmasking

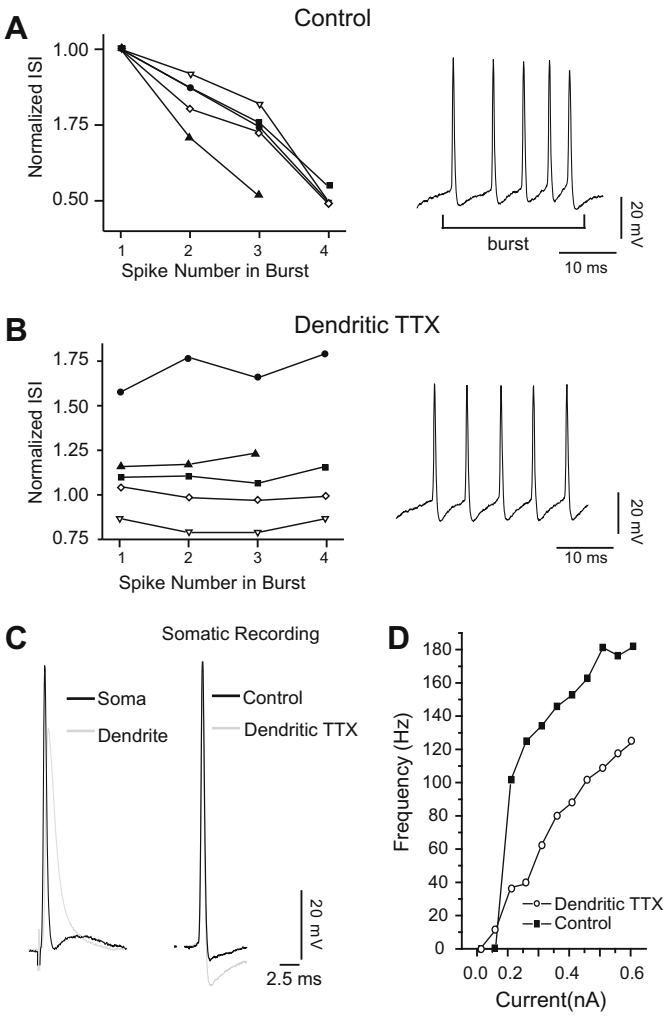

Fig. 1. An active dendrite regulates somatic firing dynamics. A,B, Plots of somatic ISI during a single burst for five separate cells recorded in control condition (A) and following focal application of TTX in dendrites (B). All ISIs in (A) and (B) are normalized to the first ISI in the control recording of (A). Each cell is represented by a different symbol. Recordings to the right of (A) and (B) are representative cases of somatic spike firing in the control and TTX condition, respectively. (C) Superimposed somatic (black) and dendritic (grey) spikes from separate recordings to show the relationship between the dendritic spike and DAP. Control recordings are shown on the left. Blockade of dendritic Na^+ channels by TTX application to the dendrites removes the somatic DAP and unmasks a large AHP (Right, grey trace) relative to control conditions (black trace), without affecting the height or shape of the somatic spike. (D) Modulation of the FI relationship by active dendritic conductances. Blockade of Na^+ conductance by dendritic TTX application (○) leads to a much shallower gain in response to step current injections when compared to control conditions (■). Modified from Fernandez et al. (2005b), Mehaffey et al. (2005).

of a large somatic AHP after eliminating the dendritic spike suggests that a significant dendro-somatic current flow exists even when a prominent DAP cannot be observed in the voltage trace. Despite the apparent lack of a DAP, the removal of the dendritic spike reveals a significant influence of the dendritic spike on the somatic voltage waveform. Further, this excitatory pulse of current from the DAP counters the intrinsic relative refractoriness of the somatic compartment, allowing a greater excitability to be observed in the somatic firing dynamics. As dendritic spikes are initiated by somatic spiking, this DAP depends on the generation of somatic spikes. Such a requirement for somatic discharge prevents the DAP from shifting rheobase, because as a spike-dependent process, it has no influence in the subthreshold regime, and can only

regulate gain after spiking has already commenced. Further, as the magnitude of this dendro-somatic current flow varies with the rate of action potential discharge in the somatic compartment, then the overall influence of the dendritic activity on somatic firing rate scales roughly multiplicatively with the output rate (Mehaffey et al., 2005). This explains why a manipulation of dendritic excitability causes a gain change rather than a simple subtractive shift in the FI curve.

3.3. Bursting is conserved across multiple species of Gymnotiform fish

Studies on the biophysics and dynamics of burst firing in the ELL have been performed primarily in *A. leptorhynchus* (Doiron et al., 2002; Fernandez et al., 2005b; Lemon and Turner, 2000; Noonan et al., 2003; Turner et al., 1994). In order to examine whether bursting can be observed across multiple species of fish, we performed in vitro slice recordings from two species of related gynmnotiform fish (*A. albifrons* and *E. virescens*). Fig. 2A shows the consensus phylogeny for the Order gymnotiformes, taken from Alves-Gomes (1999). A representative example of burst firing in *A. leptorhynchus* is shown in Fig. 2B. As described above, repetitive firing of bursts is observed above a threshold level of current injection. A similar phenotype of burst discharge can be observed in ELL pyramidal cells of the closely related species *A. albifrons* (Fig. 2C). As these two species are closely related (Fig. 2A), we also performed these experiments on a more distantly related Gymnotiform, *E. virescens*. Burst discharge was also observed in *E. virescens*, showing that burst firing is likely conserved across many wave-type electric fish (Fig. 2D). Interestingly, a similar pattern of burst discharge can be observed in *Gymnotus carapo* (Angel Caputi, personal communication), a pulse-type fish distantly related to *A. leptorhynchus*. Although conservation of the bursting phenotype does not necessarily prove conservation of the burst mechanism, it suggests that burst discharge is a common adaptation for electrosensory processing in ELL pyramidal cells.

3.4. Ionic basis for dendritic spike broadening

A crucial component defining bursting is the slow dynamics that drive the decreasing ISI during bursting. Previous work established that a critical feature driving the decrease in ISI and progression to burst firing is a dynamic dendritic spike waveform (Noonan et al., 2003). One possible explanation for the broadening of the dendritic spike during repetitive firing was a cumulative inactivation of dendritic K^+ current. Frequency-dependent spike broadening through cumulative inactivation of K^+ currents has been shown previously (Aldrich et al., 1979; Ma and Koester, 1995, 1996; Shao et al., 1999). Such a process would ensure an increase in the amount of current flow from dendrite to soma after each somatic spike. We therefore used on-cell patch-clamp recordings under DIC-IR at distances between 150 and 200 μm from the soma in order to measure the rate of K^+ current inactivation. Our voltage-clamp protocol consisted of depolarizing the dendritic patch to −19 mV (based on an established membrane resting potential of −69 mV). Recordings contained 3–6 channels per patch (Fig. 3A) (Fernandez et al., 2005b). Ensemble averages revealed that the time constant of inactivation was 1086 ± 87 ms, a time scale far too slow to be directly involved in burst generation. Although the molecular identity of these channels was not examined, a likely candidate is the Kv3 class of potassium channels, which can show inactivation on these slow time scales (Deng et al., 2005; Fernandez et al., 2003; Mehaffey et al., 2006; Rashid et al., 2001a,b), although ELL pyramidal cells express a number of other K^+ channels as well (Fernandez et al., 2005a; Smith et al., 2006). Such a slow rate of inactivation is two orders of magnitude outside the time scale of any given ISI during a burst, and is therefore unlikely to contribute significantly to spike broadening during bursting. Previous modeling studies required dendritic K^+ current to inactivate at much faster rates ($\tau_{inact} < 5$ ms) in order to reproduce dendritic spike broadening during bursting (Doiron et al., 2002, 2001b). Thus the K^+ current we measured in dendrites was an un-

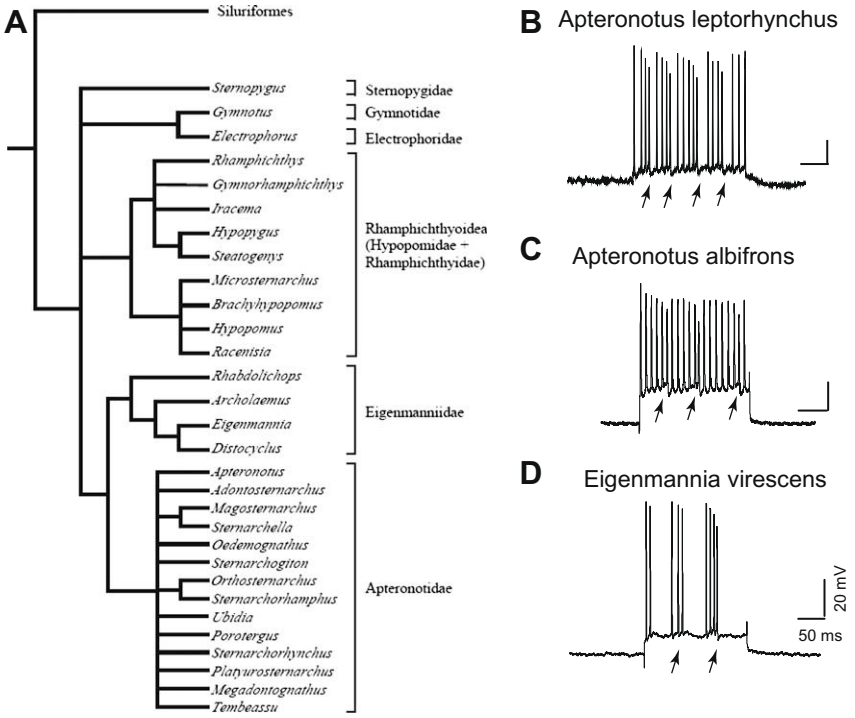

Fig. 2. Bursting is conserved across many Gymotiform species. (A) The consensus phylogeny for the Order Gymnotiformes, taken from Alves-Gomes (1999). (B) Representative example of burst firing in *A. leptorhynchus*. As described previously, repetitive firing of bursts is observed after sufficient current injection (0.45 nA). (C) A similar phenotype of burst discharge can be observed in ELL pyramidal cells recorded in the closely related species *A. albifrons* (0.7 nA). D, Representative example of bursting in the more distantly related Gymnotiform, *E. virescens* (0.25 nA). Arrows in (B–D) denote the timing of burst AHPs that signify the end of each burst.

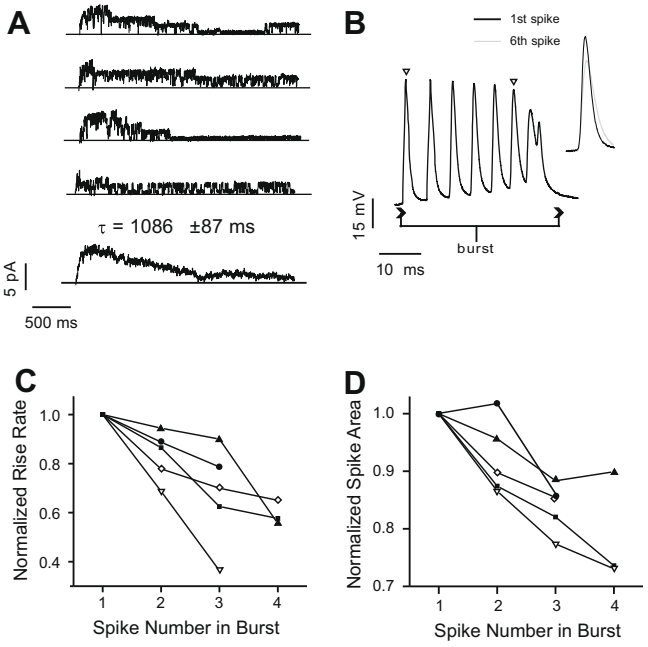

Fig. 3. Dendritic spike broadening is mediated by Na^+ current inactivation. A, Cell-attached patch recordings of K^+ channels from ELL pyramidal cell apical dendrites (150–200 μm from cell body). Membrane potential was stepped from −69 mV to −19 mV for 4 s using a step depolarization. Ensemble averages (bottom trace) were constructed by averaging 6–8 sweeps. Inactivation was fit with a single exponential decay function. B, Representative voltage trace from a dendritic recording during burst firing. The cell was depolarized until burst firing threshold was reached. *Inset* superimposes the first (black) and sixth (grey) dendritic spike for comparison. (C and D) Plots of dendritic spike rate of rise (C) and area (D) during burst firing for five separate cells. Each cell is represented by a different symbol. The last dendritic spike was not included due to contamination from the second spike of the terminating doublet. Dendritic spike rate of rise and area are normalized to the first spike in the burst. Modified from Fernandez et al. (2005b).

likely candidate for the process of dendritic spike broadening leading to burst firing (Fernandez et al., 2005b).

Alternatively, it has been established that spike broadening can also be caused through Na^+ channel inactivation (Fleidervish et al., 1996; Van Goor et al., 2000). In particular, dendritic Na^+ currents in hippocampal CA1 cells have been found to be particularly susceptible to cumulative inactivation during repetitive firing (Colbert et al., 1997; Jung et al., 1997). Sodium current inactivation reduces the rate of rise and the repolarization of the spike through a decrease in recruitment of Na^+ current that in turn affects spike height, and in turn the activation of repolarizing K^+ current. These properties in fact resemble the behaviour of ELL pyramidal cell dendritic spikes during a burst, thus suggesting cumulative Na^+ current inactivation as a candidate mechanism for spike broadening. Direct patch-clamp observation of Na^+ channels was not feasible in ELL pyramidal cells due to the low conductance of single Na^+ channels and a density below that required to provide macro-patch currents in the on-cell configuration. We were however, able to use the rate of rise and the total area underneath a dendritic spike to quantify the degree Na^+ current inactivation in dendrites. Using dendritic microelectrode recordings performed in the VML (100–150 μm from the pyramidal cell layer) we were able to drive burst firing and record dendritic spikes (Fig. 3B). The measured rate of dendritic spike rise (Fig. 3C) and the area underneath the spike (Fig. 3D) decreased as spike firing within a burst progressed. These changes could be substantial; in that study attaining up to a 60% decline in spike rate of rise within the first four spikes of a burst (Fernandez et al., 2005b).

This study strongly implicated Na^+ current inactivation as the underlying variable for spike broadening, DAP growth, and the transition to bursting (Fernandez et al., 2005b). The experiments in Fig. 3 revealed that a reduction in dendritic Na^+ current availability causes an increase in cell excitability. Note that a complete absence of Na^+ current in dendrites decreases excitability (as shown in Fig. 1D) (Mehaffey et al., 2005), while a partial inactivation paradoxically increases excitability (Fernandez et al., 2005b). This indicates that somatic excitability and dendritic Na^+ current density do not relate monotonically, but display a more complex dependency (Fernandez et al., 2005b; Mehaffey et al., 2005).

3.5. Dendritic Na^+ current inactivation causes slow burst dynamics through shifts of relative latency

An approach that has been especially valuable in the study of qualitative changes in neuronal firing patterns has been the construction of simplified mathematical models. In order to understand how a decrease in dendritic Na^+ current can paradoxically increase cell excitability, we used a simple phenomenological model, which consisted of a single compartment representing the dendrite coupled to a second compartment representing the soma (Fernandez et al., 2005b). These two compartments influenced each other reciprocally through a current term proportional to the voltage difference between the two compartments, and then scaled by terms representing the resistance between the compartments and the size of the compartments. The model contains two currents in each compartment. The soma contains a fast Na^+ current and a fast K^+ current. To reduce the dimensionality of the model we assumed that inactivation of somatic Na^+ current was directly proportional to the K^+ current and that the Na^+ activation variable equilibrated with voltage instantaneously (Rinzel, 1985). The dendritic currents consisted of a Na^+ current with slightly slower activation and inactivation kinetics relative to the soma. The K^+ current in the dendrite was independent of Na^+ current inactivation, and displayed a more positive steady-state voltage relationship than in the somatic compartment. Spike broadening in dendrites required slightly slower kinetics and a lower density of Na^+ current in the dendrites, consistent with previous studies (Colbert et al., 1997; Jung et al., 1997; Stuart and Hausser, 1994; Turner et al., 1994).

As mentioned previously, ELL pyramidal cell bursting shows a transition from tonic to burst firing as current injection increases (Lemon and Turner, 2000; Turner et al., 1994). The reduced two-compartment model reproduced this phenomenon as well as the progressive increase in amplitude through a spike train of the DAP (Fig. 4A–C). We were also able to reproduce the decrease in dendritic spike area during a burst (Fig. 4D), which was not captured by previous models (Doiron et al., 2002). The rate of rise of the dendritic spike and the extent of dendritic Na^+ current available also decreased during the build up phase of the burst. This was a key observation as it shows that an overall drop in dendritic excitability is associated with an increase in somatic excitability (Fernandez et al., 2005b). Thus our reduced phenomenological model of the ELL pyramidal cell displays the essential elements of the burst dynamics, allowing us to more carefully study the underlying processes.

3.6. Dendritic Na^+ current inactivation increases excitability by delaying the DAP

The same study determined the biophysical mechanism by which a net decrease in dendritic excitability causes an increase in somatic excitability and the resulting shift to burst firing (Fernandez et al., 2005b). We found that the loss of available dendritic Na^+ current caused a broadening of the dendritic spike as well as

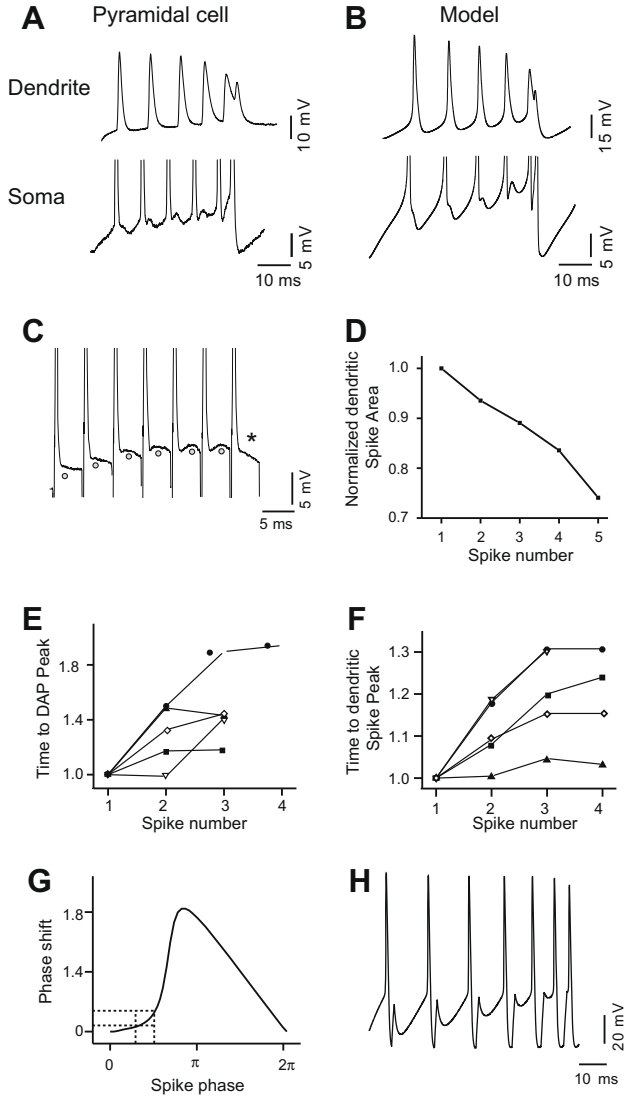

Fig. 4. Dendritic Na^+ current inactivation can increase somatic excitability by delaying the DAP. (A and B) Representative membrane voltage traces recorded in a pyramidal cell (A) dendrite (top panel) and soma (bottom panel) and in a reduced model (B). Dendritic and somatic recordings are from different cells and somatic spikes are clipped to improve visualization of the DAP. Note that the model generates the entire process leading to a burst, including an increase in DAP amplitude during repetitive firing and a terminating spike doublet, as well as evidence for a temporal shift in the peak of the DAP (compare (A and B) bottom panels). (C) Plot of dendritic spike area during burst firing in the model cell illustrates a progressive decrease in area with each spike in a burst. (D) Pyramidal cell recording from the soma during antidromic stimulation at 200 Hz. Note that the peak of the DAP (*circle*) shifts away from the somatic spike until an abrupt failure (*) signifying the loss of backpropagation. (E and F) Plots of the time to peak of the DAP (E) and dendritic spike peak (F) during antidromic stimulation for five separate cells (shown by different symbols). Antidromic stimulation frequencies varied from 140 to 200 Hz, and peak latencies were normalized to the first spike in the train. In all cells recorded the DAP and dendritic spike peak latency increased during repetitive simulation. G, Phase response curve (PRC) for model without a dendrite. Phase cycle was calculated from the peaks of the spike with 0–2π denoting the distance between two consecutive spike peaks. The phase advance was calculated as the reduction in phase cycle length compared to the control (no pulses) that was evoked with pulses (I_E = 140 μA/cm^2 for 0.42 ms) delivered at different locations in the phase cycle. H, Phase varied pulses delivered to the model and corresponding voltage response (bottom panel). Pulses arrived with increasing delay relative to the somatic spike. Each successive pulse was also reduced in height and increased in width to simulate DAP dynamics during bursting. Note that the effectiveness of the dendritic spike increases, despite the decrease in area of the pulse. Modified from Fernandez et al. (2005b).

delay in the time to reach peak. These changes could translate to a shift in the arrival of the peak DAP current at the soma (Fernandez et al., 2005b). Combined with a broader dendritic spike, this would extend the amount of time the DAP influenced the soma and thus generate both a shift in timing of the DAP peak as well as the total duration of the DAP. We measured the time to peak of the DAP or dendritic spike during repetitive antidromic stimulation, as it permits precise control of firing rate and a consistent reference point. Neither the DAP nor the dendritic spike increased in latency if the stimulus frequency was below that known to induce a shift from tonic to burst firing (~100 Hz in vitro). In this study, we were able to observe that stimulus frequencies ranging from 140–200 Hz induced distinct changes in DAP timing (Fig. 4C and E) (Fernandez et al., 2005b). With each successive spike the peak of the DAP increased in amplitude and was delayed relative to the somatic spike by 120–190% of control delays (Fig. 4E). We then recorded from dendrites during identical antidromic stimulation. In all cells measured (stimulation frequencies >140 Hz) the time to peak of the dendritic spike was delayed by 105–135% at the 4th spike (compared to the first spike, Fig. 4F).

The appearance of a larger DAP at the soma is thus due to the DAP shifting away from the somatic spike. As it also moves away from the influence of the spike AHP to arrive at a time with less repolarizing current, its influence is increased. As a framework to investigate such a change in relative timing, we considered the phase response curve (PRC) of a neuron. In essence, the PRC relates the timing of a perturbation within the spike cycle with its ability to influence the phase of the cycle (e.g., to advance or delay the next spike). A PRC is determined by transiently exciting a system at different points of the oscillation phase (Hansel et al., 1995, 1993; Rinzel and Ermentrout, 1998), and the corresponding advance or delay is measured. In the past, PRCs have been primarily considered when studying synaptic activation of neurons at different points in the spike cycle or in weakly coupled networks of neurons (Hansel et al., 1995; Reyes and Fetz, 1993). Theoretical and computational studies have shown that the qualitative shape of the PRC depends on the dynamics which underly spiking (Ermentrout, 1996; Hansel et al., 1995). If the firing arises through a saddle node on invariant cycle bifurcation, the resulting PRC is invariably positive, and the timing of the next spike can only be advanced (Ermentrout, 1996; Hansel et al., 1995). This is in contrast to settings where the oscillation arises through a sub-critical Hopf bifurcation (i.e. Hodgkin–Huxley model) and an excitatory pulse immediately following the spike delays the onset of the next spike, while later pulses advance the phase (Ermentrout, 1996; Hansel et al., 1995).

To understand the effect of DAP timing in our system in the context of a PRC we equated the arrival of the DAP at the soma to a brief excitatory current pulse. As the transition from quiescence to tonic firing is associated with a saddle node bifurcation of fixed points, the PRC should consist only of zero or positive phase advances. To confirm this we first removed the dendritic compartment from our model to measure the somatic PRC. The PRC indicates that excitatory pulses arriving immediately after the peak of the spike (phase = 0) have a minimal ability to advance the phase, while excitatory pulses arriving with a greater delay can advance the phase considerably (Fig. 4G). As a qualitative test of DAP dynamics on somatic excitability we excited the model during tonic firing at 65 Hz and added current pulses coming at different times after the peak of the somatic spike. In order to examine the effects of decreasing dendrite spike height and increasing dendritic spike width, we also made each successive excitatory pulse slightly shorter (from 140 to 90 μA/cm^2) and wider (from 0.42 to 0.52 ms), but with an overall decrease in the area (from 1 to 0.78), as observed experimentally. Despite the fact that later pulses in the train were smaller, the positive shift in location of the pulse in the phase cycle was sufficient to compensate and caused an increase in the phase advance and the resulting firing frequency.

Note that the last pulse generates a doublet and reproduces the slight drop in somatic spike height associated with doublets during bursting (Fig. 4H). Importantly, this shows that the effectiveness of the 'pulse-DAP' is increased despite the fact that the underlying current is actually smaller (Fig. 4H). Thus we were able to show that the exact timing between the somatic and dendritic spike regulates the pattern of spikes generated (Fernandez et al., 2005b). Furthermore, the relative timing of somatic and dendritic spikes changes depending on the history of spike discharge. This allows the cumulative inactivation of dendritic sodium channels to underly the patterned spike discharge observed during bursting.

3.7. Divisive gain control mediated by dendritic inhibitory regulation of the DAP

Dendritic excitability can also be regulated by synaptic inputs, with many classes of interneurons now known to synapse exclusively onto specific dendritic compartments (Soltesz, 2006). The ELL is no exception and contains many local inhibitory interneurons (Maler, 1979; Maler and Mugnaini, 1994). Two contrasting local GABAergic interneurons are notable in this regard. The type 2 granule cell (G2) interneuron receives direct electroreceptor input and projects to the pyramidal cell soma. In contrast, neurons of the ventral molecular layer (VML cells) receive descending excitatory synaptic feedback and project specifically to the region of the proximal apical dendrite which is known to actively propagate dendritic Na^+ spikes (Turner et al., 1994)(Fig. 5A). In both cases the inhibition is mediated by the $GABA_A$ receptor subtype (Berman and Maler, 1999). In order to evaluate the role of these interneurons, we performed a series of experiments mimicking their activation by focal application of a selective $GABA_A$ agonist, muscimol (Mehaffey et al., 2005). Muscimol (200 μM) was applied to either the soma (e.g., mimicking the activity of GC2 cells) or the proximal dendritic region of the pyramidal cell (e.g., the region in which VML cells synapse) while recording from the soma of ELL pyramidal cells. As before, we were able to use fibre bundles that bound the pyramidal cell layer (PCL) as barriers to the diffusion of pharmacological agents, and can therefore separate dendritic and somatic effects of applied modulators on cell output (Mehaffey et al., 2005; Noonan et al., 2003; Turner et al., 1994).

Pharmacological activation of dendritic $GABA_A$ receptors led to a divisive effect on the FI relationship, with minimal effects on the rheobase at which firing commenced (Fig. 5B). Linear fits from the rheobase to the saturation point of the FI curve revealed a significant mean decrease in slope, meaning an overall reduction of the output gain. The rheobase for initial spiking did not change significantly, with a mean change of 0.08 ± 0.07 nA. This lack of a subtractive influence is due to the site of inhibition being too distal to the spiking mechanism, a result we were able to confirm with a multicompartmental model (Mehaffey et al., 2005). To ensure divisive effects were not due to the diffusion of pharmacological agents during the recording of individual FI curves, repeated recordings were made after the dendritic muscimol ejection. The divisive effects described were reproduced over multiple recordings, indicating that the changes within a single FI curve were not due to diffusion during the course of recording.

In contrast to dendritic application, somatic application of muscimol caused a subtractive effect on FI curves (Fig. 5C). These experiments showed that somatic muscimol application did not lead to a reduction in slope of the FI relationship, but did shift the rheobase for tonic spiking (Fig. 5C). Such distinct effects of muscimol depending on the spatial extent of its application suggests distinct computational properties of dendritic versus somatic inhibition in our cells: dendritic inhibition has a divisive effect while somatic inhibition has subtractive effects (Mehaffey et al., 2005). Such divisive effects could play important roles in burst coding, allowing regulation of burst ISIs while leaving isolated spikes unaltered (Doiron et al., 2007; Oswald et al., 2007).

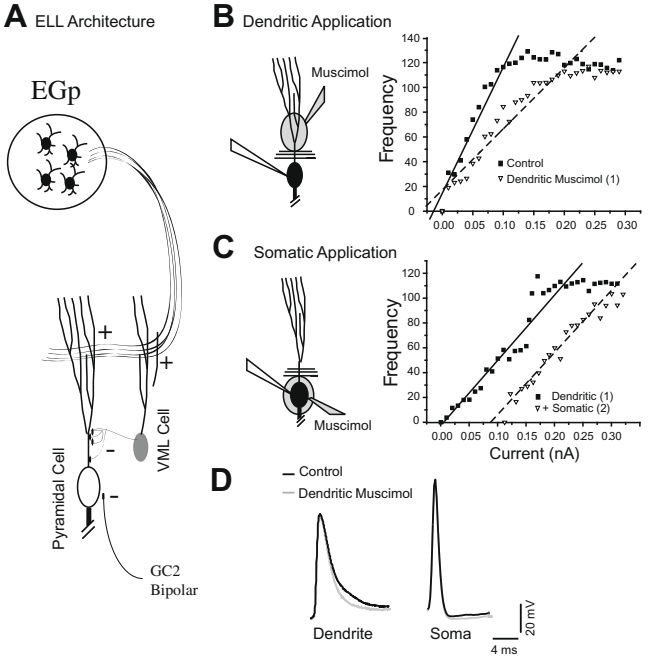

Fig. 5. Dendritic inhibitory conductances modulate gain divisively through regulation of the DAP. (A) Simplified architecture of ELL indirect feedback pathway. Parallel fibre feedback of EGp cerebellar granule cells drive both the pyramidal cell (white) and VML cell (grey). The VML cell gives rise to inhibitory synapses contacting pyramidal cell apical dendrites while inhibitory inputs to the pyramidal cell soma arise in part from GABAergic granule cells (GC2) (Berman and Maler, 1999). (B) Focal application of the $GABA_A$ agonist muscimol (200 μM) to the apical dendrites (▼, *dashed line*) causes a divisive shift in the FI relationship relative to control (■, *solid line*) without significantly affecting the rheobase to spiking. (C) Application of muscimol to the soma subsequent to dendritic ejection (▼, *dashed line*) fails to further divide the FI curve obtained after dendritic muscimol (■, *solid line*), having instead a subtractive effect. (D) Application of muscimol to the soma in a separate recording does not shift the slope of the FI curve (▼, *dashed line*), but shifts the spike rheobase relative to control conditions (■, *solid line*). Lines in (B) and (C) are linear fits to the FI plot between rheobase and peak firing frequency. All FI plots have been normalized such that control rheobase is zero. (D) Application of muscimol to the apical dendrites while recording from dendrites reveals a reduction in the width of the base of the dendritic spike. This reduction in dendritic spike width is correlated with a larger somatic AHP (grey) relative to control conditions (black) in separate somatic recordings. Data from Mehaffey et al. (2005).

3.8. The contribution of the DAP can be regulated by dendritic leak conductances

As we discuss above, in our system (and in many others) the DAP depends on active dendritic conductances (Larkum et al., 1996; Magee and Carruth, 1999; Turner et al., 1994). In order to examine the mechanism underlying the gain changes observed after dendritic muscimol application, recordings were made from the proximal dendrites of pyramidal cells during dendritic application of muscimol (Mehaffey et al., 2005). After muscimol ejection, the rate of repolarization of the dendritic spikes was noticeably faster (Fig. 5D). This reduction of the dendritic spike was observed in separate somatic recordings as a larger AHP following repolarization, indicating a smaller DAP (Fig. 5D). Analysis of the AHPs recorded somatically following dendritic muscimol ejection revealed that under control conditions, the mean AHP size increased by 35%. This showed that an increase in the rate of repolarization of the dendritic spike by muscimol was able to down-regulate the influence of the DAP on the somatic membrane voltage, unmasking a larger AHP.

In comparison, ejections of muscimol to the cell body layer (PCL) did not create a significant change in AHP size, indicating that the effect of the DAP was unchanged. Consistent with the inherent multiplicative effect of the DAP, somatic muscimol ejection did not produce divisive effects, but did cause a subtractive change in rheobase for the FI curve. Thus dendritic, but not somatic, muscimol application affects the width of the dendritic spike and subsequently, the size of the somatic AHP. Therefore the somatic AHP and the resulting gain is regulated by a balance between somatic AHP generating currents, and a positive dendro-somatic current flow. This regulation of the AHP by the DAP is a property exclusive to the apical dendrites of the cell (Mehaffey et al., 2005; Turner et al., 1994). Therefore changes in dendritic leak are capable of producing a divisive change in gain, allowing the VML cell to regulate the gain of pyramidal cell spike discharge (Mehaffey et al., 2005; Turner et al., 1994). This allows for a deterministic regulation of the gain, a process that contrasts with many gain control mechanisms that require stochastic fluctuations in the synaptic drive (Chance et al., 2002; Mitchell and Silver, 2003; Prescott and De Koninck, 2003). Intuitively, such noise can degrade the accurate processing of sensory stimuli, and may be deleterious in the early stages of sensory processing.

3.9. Distinct subtypes of dendritic inhibition have distinct effects on the DAP

Pyramidal cells of the ELL receive synaptic modulation from other nuclei as well as from local interneurons. One particular pathway involves a direct inhibitory feedback from the nucleus praeeminentalis (nP). Briefly, pyramidal cells drive bipolar cells of the nP which in turn send inhibitory (GABAergic) fibers back to the ELL through the tractus stratum fibrosum (StF) (Berman and Maler, 1999; Maler and Mugnaini, 1994) (Fig. 6A). This pathway is known to activate both $GABA_A$ and $GABA_B$ receptor-mediated IPSPs causing inhibition due to Cl^- and K^+ conductances in pyramidal cells, respectively (Berman and Maler, 1998b). The observed currents are due to synaptic contacts onto the somata and proximal apical dendrites of basilar and non-basilar pyramidal cells (Maler and Mugnaini, 1994) (Fig. 6A). The fast $GABA_A$ conductance arising from bipolar cells can induce a gamma frequency oscillation in pyramidal cells due to negative feedback recruited when the fish is exposed to electric fields with a spatial configuration similar to electrocommunication signals (Doiron et al., 2003, 2004; Lindner et al., 2005). The gamma oscillation evoked by this input is ~30–50 Hz, while the $GABA_B$ currents recorded in pyramidal cells have a duration of ~500 ms (Berman and Maler, 1998b), far too slow to be involved in generating the oscillation. The role of the slow $GABA_B$ component of this feedback pathway has only recently begun to be studied (Mehaffey et al., 2007).

With sufficient current injection, many pyramidal cells display the distinctive bursting described above (Fig. 6B). We can quantify the propensity towards bursting by calculating the range of current injections between the initiation of spiking and the initiation of bursting (e.g., the tonic range of firing, Fig. 6C). In order to specifically examine the effects of $GABA_B$ activation we applied baclofen (100 μM), a selective $GABA_B$ agonist, to the PCL through focal pressure ejection from a small tipped pipette. Note that because GABAergic afferent axons from nP bipolar cells travel along the ventral StF, we could not use the StF as a barrier in this case to segregate somatic and dendritic effects of ejected drugs as in previous studies (Mehaffey et al., 2005; Noonan et al., 2003; Turner et al., 1994).

Pressure ejections of baclofen in the PCL rapidly evoked either a decrease or a complete elimination of the tonic firing range of ELL pyramidal cells. Instead, cells repetitively fired spike doublets rather than exhibiting the normal range of tonic firing (Fig. 6B2). Fig. 6D shows a representative FI plot displaying the full range of firing behaviours before and after baclofen ejections. As current injection increased in control conditions, pyramidal cells fired at an increased rate and eventually began to burst. After baclofen ejection the tonic range of firing was abolished, such that the cell began to burst immediately upon crossing rheobase (Fig. 6B–D). Not all cells showed a direct transition to bursting, but all pyrami-

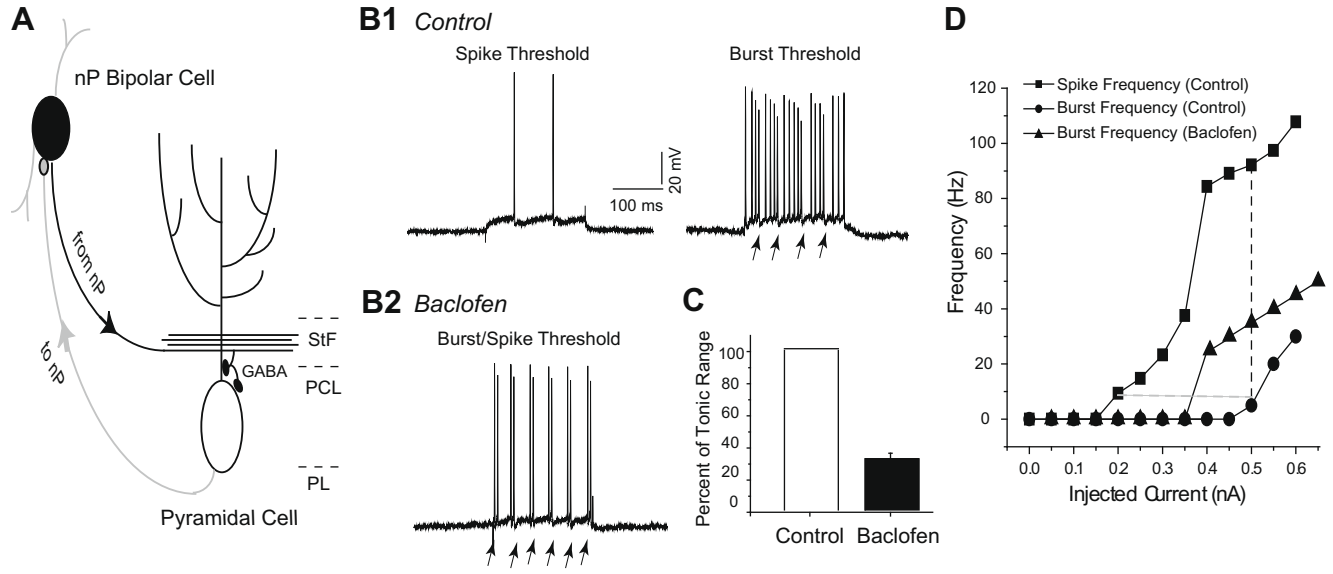

Fig. 6. A direct inhibitory feedback pathway can regulate bursting. (A) Schematic diagram of the direct feedback pathway to the ELL. Pyramidal cell axons project to nP bipolar cells, which in turn synapse on the pyramidal cell near the soma and along the most proximal apical dendritic region, activating both $GABA_A$ and $GABA_B$ receptor subtypes. (B) Pyramidal cells fire tonically in response to current injection (B1, *left*, 0.2 nA). When the injected current surpasses a second threshold value the cell responds with patterned bursting (B1, *right*, 0.5 nA; *arrows* denote burst AHPs). Baclofen application to the soma/proximal dendritic region activates $GABA_B$ receptors and the pyramidal cell now responds with spike doublets immediately after crossing spike threshold with no initial tonic firing (B2, 0.4 nA). (C) Baclofen leads to a compression of the tonic range of firing, as indicated by a significant decrease in the range of current injections between spike threshold and bursting. (D) Plots of the *F–I* relationship for tonic and burst discharge in a representative cell before and after focal pressure application of baclofen. *Dashed lines* indicate burst threshold (*black*), and the tonic firing range (*grey*) in control conditions. Data from Mehaffey et al. (2007).

dal cells displayed a compression of the tonic firing regime, with an average 69 ± 5% decrease in the tonic range of firing (Fig. 6C). Cell fills revealed that this behaviour could be observed in both basilar and non-basilar classes of pyramidal cells. Further, upon activation of inhibitory receptors by baclofen, there was a corresponding increase in rheobase – e.g., a subtractive shift in the FI plot. This is consistent with the predicted effects of inhibition discussed above; however the compression of the burst firing regime is distinct from the effects of inhibition. In most cells, inhibition leads to a subtractive change in rheobase, but does not alter the firing dynamics of the cell (e.g., (Mehaffey et al., 2005; Ulrich, 2003). In this case, for a fixed value of static depolarization, dendritic $GABA_B$ inhibition was able to qualitatively alter the firing behaviour of ELL pyramidal cells, a non-linear interaction not predicted by simple subtractive inhibition.

3.10. A reduced model explains how dendritic $GABA_B$ receptor activation can regulate bursting

We were able to use the reduced two-compartment model described above (Fernandez et al., 2005b) to examine the possible mechanisms underlying $GABA_B$ regulation of burst dynamics. Under control conditions, the model cell fires individual spikes (Fig. 7A). Applying dendritic $GABA_B$-like inhibition was capable of replicating the decrease in tonic range of firing and the transition to a pure "doublet" mode of firing (Fig. 7B). Our model thus suggests that the $GABA_B$ induced compression of the tonic firing range seen experimentally is due specifically to inhibition of the apical dendrite. This suggested that compression of the tonic firing regime recorded in vitro was due to activation of dendritic $GABA_B$ receptors from the nP bipolar cell feedback pathway.

The change in the dynamics of pyramidal cell output invoked by dendritic $GABA_B$ conductances could be explained by considering the normal dynamics of bursting (see Sections 3.1 and 3.3). Normally, spikes in ELL pyramidal cells are initiated near or at the soma and backpropagate along the apical dendrite. The dendritic spike is broader and is delayed relative to the somatic spike. The resulting voltage discrepancy between the somatic and dendritic compartments causes a dendro-somatic current flow (e.g., the DAP, Fig. 7C). Spike doublets normally result when repetitive firing promotes a gradual shift in the dendritic spike rate of rise due to Na^+ channel inactivation, delaying the dendro-somatic current

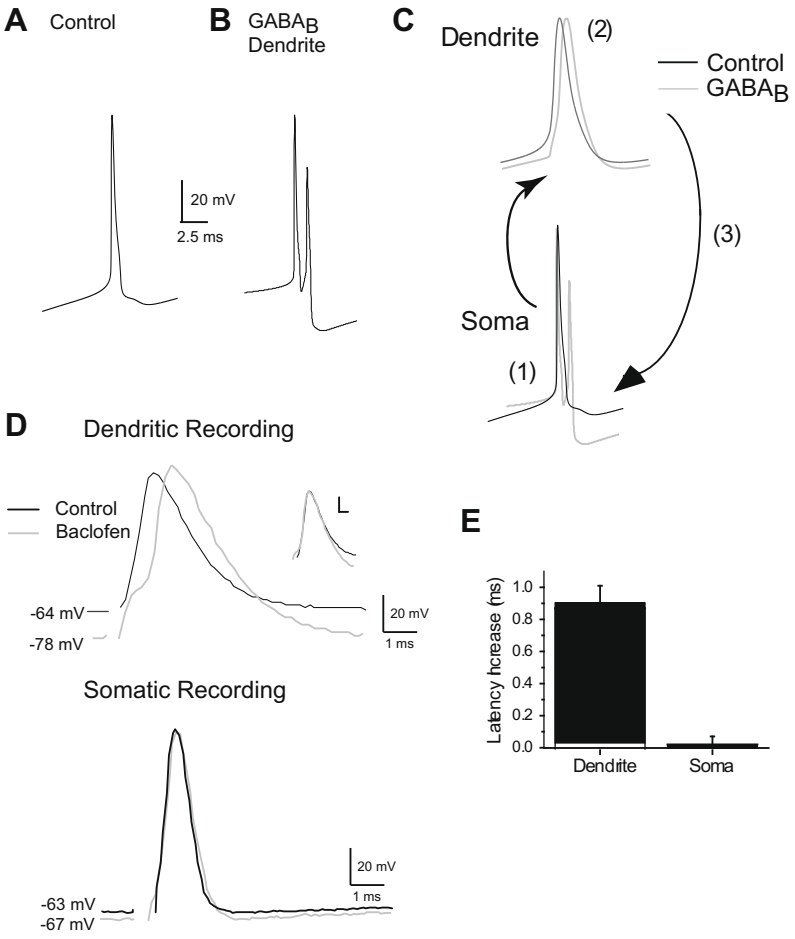

Fig. 7. $GABA_B$ receptor activation regulates dendritic spike latency and somatic firing dynamics. A, Somatic spike in the model under control conditions ($g_{s,dGABAb}$ = 0 mS/cm^2). (B) When $GABA_B$ currents are added to the dendritic compartment (g_{dGABAb} = 0.4 mS/cm^2) the cell develops spike doublets, replicating the results seen after baclofen application to pyramidal cells in vitro. (C) In the model the addition of either $GABA_B$ current (shown here) or dendritic hyperpolarization delays the dendritic spike (2) relative to the somatic spike (1), suggesting that dendritic hyperpolarization is sufficient to regulate bursting. Either manipulation shifts the dendro-somatic feedback underlying a DAP (3) further outside the somatic refractory period, allowing the generation of a second somatic spike that signifies the transition to burst output. D, Superimposed representative recordings of antidromic dendritic or somatic spikes before and after pressure application of baclofen (100 μM) in the PCL. Baclofen induces a membrane hyperpolarization at dendritic sites and a pronounced increase in the delay of dendritic spike onset and peak latency with no change in spike rate of rise. By comparison, baclofen has little effect on somatic membrane potential, spike latency or rate of rise. *Inset* shows superimposed control and test dendritic spikes aligned for comparison of spike rate of rise. Stimulus artefacts are truncated. E, Plot of average peak latency of dendritic or somatic spikes before and after baclofen application, showing that spike latency is selectively increased in the dendrite. Data from Mehaffey et al. (2007).

flow sufficiently such that the DAP falls outside of the somatic refractory period, causing a second somatic spike (Fig. 7C) (Fernandez et al., 2005b).

We were able to confirm the model predictions by making recordings from pyramidal cell proximal dendrites near or within the StF. Under control conditions the dendrite had a mean resting potential of −64.5 ± 1.1 mV. After application of baclofen, the dendrite hyperpolarized to −81.4 ± 1.8 mV (Fig. 7D), a total hyperpolarization of 16.9 ± 2.9 mV. The hyperpolarization occurred along with an increase in latency of 0.87 ± 0.14 ms between antidromic stimulation and the peak of the dendritic spike. This shift in dendritic spike latency was not accompanied by a decrease in the rate of rise of the evoked spike. In comparison, the soma hyperpolarized by only 4.7 ± 1.5 mV, consistent with the degree of somatic hyperpolarization observed during stimulation of the inhibitory StF feedback pathway (Berman and Maler, 1998b; Mehaffey et al., 2007). In addition, the antidromically generated spike recorded somatically did not display a significant change in delay (0.02 ± 0.05 ms of control, Fig. 7D), confirming that baclofen is insufficient to delay the somatic spike, and yet has a substantial effect on dendritic spike latency.

Taken together, the experimental and modeling results suggest that $GABA_B$ activation in pyramidal cells leads to a selective hyperpolarization of the dendritic compartment, which in turn delays the dendritic spike relative to the somatic spike. By increasing the relative delay between somatic and dendritic spikes, the back-propagating spike can immediately transition the cell to burst firing. This is in distinct contrast to the actions of dendritic $GABA_A$ agonists, which did not regulate bursting, but instead lowered the gain of the firing dynamics.

3.11. $GABA_B$ inhibition can regulate bursting and therefore sensory coding

As $GABA_B$ activation was able to regulate bursting in response to step depolarizations, we tested the effects of burst regulation on coding of complex inputs in ELL pyramidal cells in vitro. This was accomplished by activating $GABA_B$ receptors with pressure ejections of baclofen while driving the cells with stimulus protocols consisting of a frozen random-amplitude modulated (RAM) stimulus low-pass filtered to contain power from 0–60 Hz. The membrane voltage of pyramidal cells during in vivo recordings track 0–60 Hz EOD AM modulations (Chacron et al., 2003; Middleton et al., 2006), a frequency content that contains power at values expected to correlate with both prey/environmental signals and conspecific signals (MacIver et al., 2001; Zupanc et al., 2006). Analysis of the pyramidal cell spike train in response to intracellular RAMs allows us to calculate the coherence (see Section 2) between a known stimulus and the resulting spike train. The resulting coherence gives a correlation function in the frequency domain allowing quantification of the amount of a stimulus successfully encoded by a neuron.

As shown previously (Oswald et al., 2004), our study (Mehaffey et al., 2007) showed that a pyramidal cell's response in vitro to a RAM under control conditions shows an overall broadband coherence to the stimulus when the combined output of isolated and burst spikes are considered (Fig. 8A). The specific responses of isolated or burst spikes can then be parsed out for separate consideration as performed for the model. This analysis showed that the response of isolated spikes encompasses a relatively broad band, or slightly high-pass, component with a small peak in power at ~40 Hz (Fig. 8A). In contrast, burst spikes instead show a preferential coherence to lower frequency components with a peak power ~10 Hz (Fig. 8A).

We then observed that after baclofen application compressed the tonic range of firing, there was a small increase in burst coherence at high frequencies. However, the more obvious effect was the reduction in the coherence between isolated spikes and low-frequency inputs (Fig. 8B). We quantified this by comparing the mean coherence for 0–20 Hz (defined as low frequency) and for 30–50 Hz (defined as high frequency) before and after baclofen to activate the $GABA_B$ receptor mediated conductance. The coherence between bursts and high-frequency events showed a modest but significant increase, while coherence between bursts and low-frequency events did not significantly change. The coherence between isolated spikes and high-frequency events did not change significantly (Fig. 8B). Rather, the most significant change was in the coherence between isolated spikes and low-frequency events, which decreased by 47 ± 6% relative to control values (Fig. 8B). We then calculated the burst fraction as the percentage of bursts relative to the total number of spikes. Baclofen also induced a significant increase in the burst fraction. Thus, the observed increase in bursting caused a redistribution of the stimulus–response coherence between bursts and isolated spikes. This allowed an overall

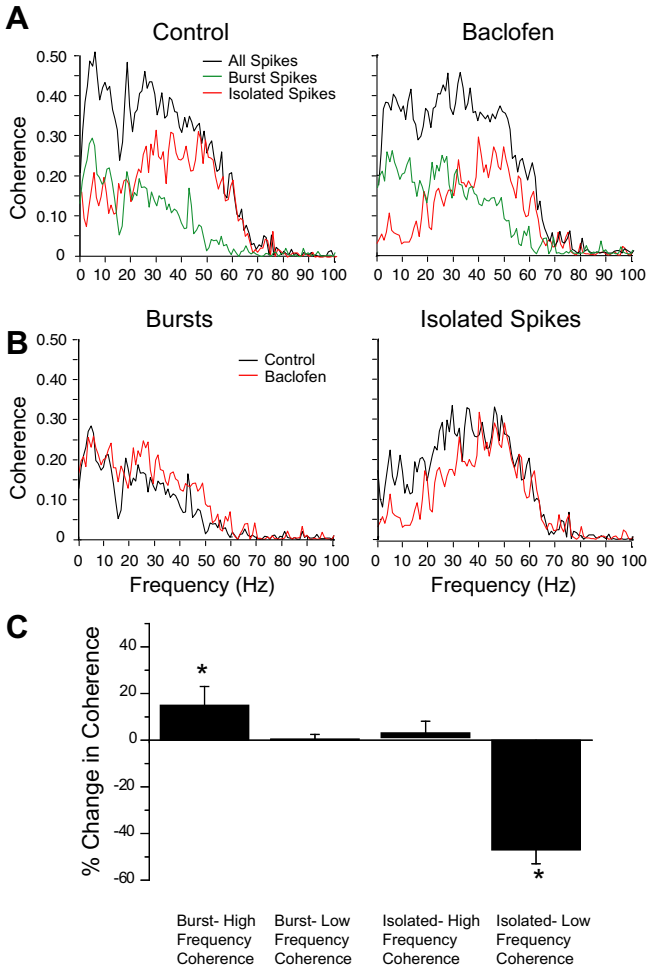

Fig. 8. Regulation of burst dynamics modifies coding properties of ELL pyramidal cells. (A) Application of baclofen to a pyramidal cell in vitro causes a shift in firing properties that matches that in the model–the coherence of bursts is slightly increased (green trace) and the low-frequency component of the isolated spike coherence (red trace) is reduced. Note that the overall coherence for all spikes (black trace) is minimally affected. (B) Control coherence (black trace) versus coherence observed when the tonic firing range is reduced by baclofen (red trace) for burst spikes (left panel) and isolated spikes (right panel) are plotted for comparison. C, Percent change in the mean coherence for high (30–50 Hz) and low (0–20 Hz) frequency stimulus components and bursts or isolated spikes. Taken from Mehaffey et al. (2007). (For interpretation of the references to colour in this figure legend, the reader is referred to the web version of this article.)

greater segregation of separate components of complex stimuli, as although burst coherence increased slightly, the predominant effect was that isolated spikes were far more selective for high frequencies (summarized in Fig. 8C). This segregation of components occurs without a suppression of the background signal, but instead uses parallel processing of separate stimulus components with distinct patterns of spikes.

4. Discussion

4.1. Mechanism of burst firing in ELL pyramidal cells

It has been well established that ELL pyramidal cells display a characteristic form of bursting, and that this bursting is driven by the dendritic spike. This bursting, at least phenomenologically, is conserved across many commonly studied species of Gymnotiform fish, including *A. leptorhynchus*, *A. albifrons*, and *Eigenmannia virescens*. Our recent work has established that the slow wind-up during the burst is driven by a gradual inactivation of dendritic Na^+ channels. Paradoxically, this decrease in dendritic excitability is able to drive an increase in somatic excitability, as reflected in both a decrease in ISI and shift to burst output.

This change in excitability is primarily due to a decrease in the rate of rise of the dendritic spike during repetitive discharge, which shifts the DAP further outside the relative refractory period of the somatic spike. The increase in the relative latency of the somatic and dendritic spike allows the DAP to be more effective, despite a decrease in the size of the dendritic spike that underlies it. The gradual increase in DAP amplitude enhances somatic excitability until a somatic spike occurs within the refractory period of the dendritic spike during a spike doublet. At this point the backpropagation of a dendritic spike is prevented and the burst is reset. As we have recently shown, this entire process can be explained and modeled solely with dendritic Na^+ channel inactivation. Interestingly, this work led to the counterintuitive result that weak, incomplete blockade of dendritic Na^+ currents could increase the excitability of the cell (Fernandez et al., 2005b). This is in stark contrast to the effects of complete blockade of the dendritic spike, which dramatically reduces the excitability of the cell.

4.2. Gain Control by regulation of the DAP

A number of studies have determined possible mechanisms to control the gain of an individual cell. Dynamic clamp (Chance et al., 2002; Mitchell and Silver, 2003) and modeling of various configurations of synaptic input (Burkitt et al., 2003; Doiron et al., 2001a; Longtin et al., 2002; Murphy and Miller, 2003; Prescott and De Koninck, 2003; Salinas and Sejnowski, 2000; Tiesinga et al., 2000) have shown how noise is capable of generating divisive effects. These studies indicate FI curves have a stationary input threshold for initial spiking (rheobase), while the gain of cell output (Hz/nA) decreases with both increasing inhibition or balanced excitation and inhibition, giving an overall division of firing rate relative to current injection. However, studies of such a noise-induced gain have used the variance in membrane fluctuation to drive spiking in a probabilistic fashion, suggesting that as that window of measurement decreases, the likelihood of successfully encoding inputs may be reduced.

In the ELL, specific forms of inhibitory input can regulate gain in a deterministic fashion. Inhibitory VML cells display a specific pattern of synaptic contacts by selectively projecting GABAergic inputs to the region of the pyramidal cell apical dendrite involved in generating the DAP. These inputs show a diminishing distribution along the proximal dendritic axis, showing a gradient of synaptic density which peaks approximately 100 μm from the soma and decays to less than 5% of contacts in regions near the soma (Maler and Mugnaini, 1994; Maler et al., 1981). This pattern of connectivity contrasts with other sources of inhibition, in which inhibitory synaptic terminals are targeted to either somatic membrane (granular cells and bipolar cells) or more distal dendritic branches (stellate cells) (Maler and Mugnaini, 1994). The specific spatial pattern of VML cell inhibition allows these cells to modify gain in a deterministic fashion through regulation of the DAP. This DAP is inherently multiplicative to output firing rate and is generated by the backpropagating dendritic spike. Inhibitory regulation of this dendritic spike is therefore able to dilute the multiplicative effect of the dendrite, reducing pyramidal cell gain. Recent work has elucidated the role of the burst ISI in coding for the amplitude of low-frequency events (Oswald et al., 2007), and theoretical work has suggested that regulation of the DAP is capable of modulating this code (Doiron et al., 2007). The possible regulation of burst coding by this mechanism is notably distinct from the $GABA_B$ synaptic mechanism described below.

4.3. Functions of somatic and dendritic GABA receptor activation

The effects of inhibition on ELL pyramidal cell spike output are complex. For instance, as described above, $GABA_A$ inhibition can cause subtractive or divisive effects on cell output depending on the location of the synapses (Mehaffey et al., 2005). However, the proximal apical dendritic $GABA_B$ receptors (but not $GABA_A$) can selectively regulate burst dynamics in relation to activity in a specific feedback pathway. It is thus important to consider not only the type and time scale of inhibition, but also the site of synaptic termination to understand the effects of inhibition on both total synaptic input and the cell's intrinsic firing dynamics.

Differential impacts of somatic and dendritic inhibition on the electrophysiological behaviour of neurons have been reported previously (Mehaffey et al., 2005; Vu and Krasne, 1992) and may allow different sets of inhibitory interneurons to selectively regulate patterns of spike generation. The activation of $GABA_A$ and $GABA_B$ receptors on the dendrite have very distinct effects. $GABA_A$ receptor activation only reduced the late phase of the dendritic spike, while $GABA_B$ conductances increased the relative latency of the dendritic spike. The apparent lack of effect by $GABA_B$ receptors on the late phase of the dendritic spike may simply reflect the more active components of spike discharge in proximal dendritic regions. In contrast, the more distal dendritic $GABA_A$ ($\sim$100 μm) conductances appear better able to regulate the shape of the backpropagating spike with less of an effect on rheobase or firing dynamics. Proximal $GABA_B$ inhibition may be unable to sufficiently regulate the more narrow dendritic spike waveform inherent to proximal regions of the dendrite, preventing the decrease in gain seen with $GABA_A$ agonists.

4.4. Synaptic regulation of backpropagating dendritic spikes

We summarize these results in the context of ELL anatomy in Fig. 9. $GABA_A$ inhibition can regulate excitability of ELL pyramidal cells in distinct fashions based on the site of inhibition. A backpropagating dendritic spike, and hence the DAP, can be regulated by dendritic inhibition mediated by the VML cell (Fig. 9, green)[3], and allows a divisive modulation of the gain. In contrast, somatic inhibition through the feedforward GC2 inhibitory interneurons can subtractively modulate the gain (Fig. 9, black). Thus the inhibitory current mediated by $GABA_A$ receptors can have dramatically different effects depending upon their spatial localization. In contrast,

[3] For interpretation of color in Fig. 9, the reader is referred to the web version of this article.

$GABA_B$ receptor mediated currents generated by inputs from nP bipolar cells, can regulate burst dynamics (Fig. 9, blue). This can in turn regulate the tuning of the spiking response of ELL pyramidal cells to complex inputs, allowing a sharper distinction between bursts and isolated spikes.

One further network effect predicted by the anatomy of the ELL (Maler and Mugnaini, 1994) involves the inhibition of VML cells (Berman and Maler, 1998a). Previous studies suggest that nP bipolar cells provide input to VML cell somata (Maler and Mugnaini, 1994). Since VML cell mediated inhibition reduces the gain of pyramidal cells (Mehaffey et al., 2005) inhibition of this interneuron should, in turn, increase the gain of pyramidal cells. We have not yet examined the possible interactions in detail, and these will depend crucially on the kinetics and subtypes of inhibitory receptors on the VML cell. Little is known of the in vivo firing behaviour of VML cells, although in vitro they can fire rapidly (>200 Hz, WH Mehaffey, unpublished observation). The synaptic dynamics will also play an important role, both for the VML cell, and for the parallel fibres that provide much of their excitatory drive. Parallel fibre to ELL pyramidal cell synapses show complex dynamics (Lewis and Maler, 2002, 2004), which may also influence VML behaviour. In contrast, bipolar cells are known to be preferentially recruited by appropriate, spatially coherent input (Doiron et al., 2003), although their synaptic dynamics again remain unknown. The complexity of synaptic interactions with intrinsic firing dynamics can only increase as short term synaptic dynamics (Lewis and Maler, 2002, 2004), feedback delays (Doiron et al., 2003, 2004; Lindner et al., 2005), and receptor subtype and spatial distribution (Mehaffey et al., 2005, 2007) are taken into account.

4.5. Generality of the dendritic influence on spike and burst coding

In response to broadband dynamic inputs ELL pyramidal cell bursts obtained both in vivo and in vitro rarely involve more than two spikes(Gabbiani et al., 1996; Mehaffey et al., 2006; Oswald et al., 2004, 2007). This is qualitatively distinct from than the multi-spike burst dynamics identified by injection of static depolarizing current (cf. Fig. 4). It has recently been shown that broadband (0–60 Hz, 0–200 Hz) dynamic stimuli may interrupt the slow dynamics of the burst seen in response to static or slow inputs (~10 Hz and less) (Doiron et al., 2007). This range of optimal frequencies suggests bursts may be an important response to low frequencies, including the JAR, environmental, and prey-like electrosensory stimuli. Interestingly, some recent results suggest that bursting is more common in the centromedial segment of the ELL, which is known to be vital for the JAR (Metzner and Juranek, 1997), but less common in the lateral segment (Mehaffey et al., 2008) which contributes to communication behaviours (Metzner and Juranek, 1997). Nevertheless, modeling results show that the influence of the DAP on spike discharge remains critical to account for the burst response to fast transients as well (Doiron et al., 2007). Fig. 8 clearly demonstrates that $GABA_B$ mechanisms that manipulate burst response in static input scenarios (cf. Figs. 6 and 7) retain their influence on the burst response to dynamic inputs. This is due to the synaptic inputs influencing the shape and timing of an individual dendritic spike, and hence the DAP, rather than the slow dynamics that lead to DAP potentiation or a gradual shift of DAP timing. Thus, while the burst response to static inputs of ELL pyramidal neurons may be somewhat unique, the response of the same cells to dynamic inputs and the regulation of this response by selective inhibition to dendrites may be a general coding strategy of a wide variety of neurons in the CNS, requisite only on dendritic excitability. While we focus here on fast synaptic regulation, both intrinsic conductances and slower neuromodulatory inputs can also play significant roles in burst regulation (Mehaffey et al., 2008).

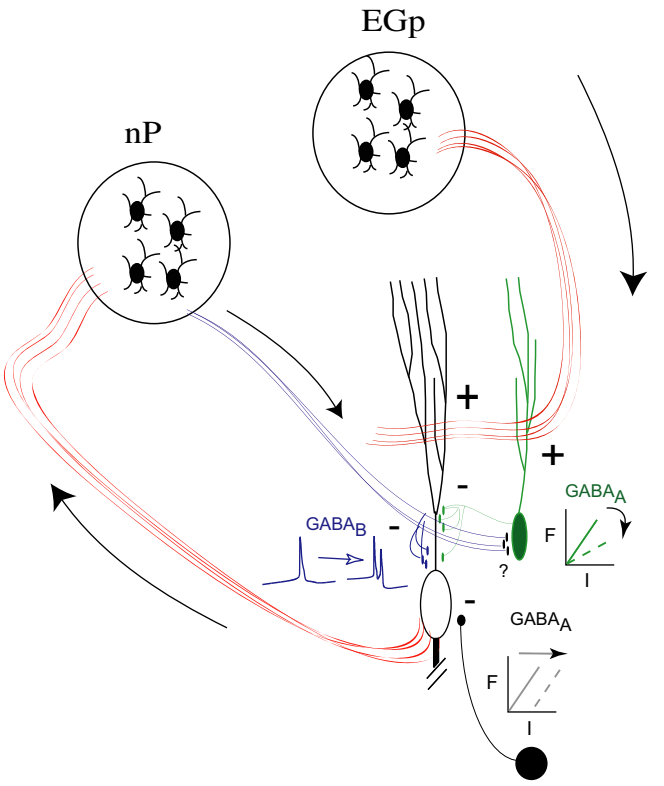

Fig. 9. Summary of feedforward and feedback pathways influencing spiking in ELL pyramidal cells. $GABA_A$ inhibition can regulate excitability of ELL pyramidal cells in distinct fashions based on the site of inhibition. Divisive modulation of gain can be accomplished by regulating the backpropagating dendritic spike. This is due to dendritic inhibition mediated by the VML cell (green). In contrast, somatic inhibition through the feedforward GC2 inhibitory interneurons can only modulate the gain in a subtractive fashion (black). In contrast, $GABA_B$ receptor mediated currents from the bipolar cells of the nP can regulate burst dynamics by modifying the temporal relationship between somatic and dendritic spike discharge (blue). The interaction between these pathways remains to be examined, but the anatomy shows that the VML cell also receives bipolar cell inhibition, suggesting a further means for GABAergic inputs to modulate pyramidal cell burst output.

4.6. Dendritic regulation of somatic excitability

The common element throughout these studies is the dendritic regulation of somatic excitability. The soma and axon are the key regions of spike initiation for the propagation of action potentials throughout the nervous system, an integral component of any Neural computation. As we emphasize here, the dendrite can play a significant role in regulating these dynamics. Repetitive activation can change somatic excitability (Fernandez et al., 2005b), and dendritic inhibition can have drastically different roles depending on their termination site and receptor subtype activated (Mehaffey et al., 2005). Thus, although a backpropagating dendritic spike clearly plays an important role in plasticity (Froemke et al., 2005; Gomez et al., 2005; Sawtell et al., 2007; Sjostrom and Hausser, 2006) and many other processes (Reyes, 2001), it also generates a 'reflection' back to the soma, which influences spike discharge and the coding properties of a cell.

Acknowledgments

We thank M. Kruskic for technical assistance. Funding was provided by CIHR operating grants (L.M., R.W.T) and CIHR studentships (W.H.M., F.R.F.), AHFMR studentship (W.H.M.) and HFSP (B.D.). B.D. is a longterm fellow of HSFP and R.W.T. is an AHFMR Scientist.

References

Aldrich Jr., R.W., Getting, P.A., Thompson, S.H., 1979. Mechanism of frequency-dependent broadening of molluscan neurone soma spikes. J. Physiol. 291, 531–544.

Alves-Gomes, J.A., 1999. Systematic biology of gymnotiform and mormyriform electric fishes: phylogenetic relationships, molecular clocks and rates of evolution in the mitochondrial rRNA genes. J. Exp. Biol. 202, 1167–1183.

Berman, N.J., Maler, L., 1998a. Distal versus proximal inhibitory shaping of feedback excitation in the electrosensory lateral line lobe: implications for sensory filtering. J. Neurophysiol. 80, 3214–3232.

Berman, N.J., Maler, L., 1998b. Interaction of GABAB-mediated inhibition with voltage-gated currents of pyramidal cells: computational mechanism of a sensory searchlight. J. Neurophysiol. 80, 3197–3213.

Berman, N.J., Maler, L., 1999. Neural architecture of the electrosensory lateral line lobe: adaptations for coincidence detection, a sensory searchlight and frequency-dependent adaptive filtering. J. Exp. Biol. 202, 1243–1253.

Burkitt, A.N., Meffin, H., Grayden, D.B., 2003. Study of neuronal gain in a conductance-based leaky integrate-and-fire neuron model with balanced excitatory and inhibitory synaptic input. Biol. Cyber. 89, 119–125.

Chacron, M.J., Doiron, B., Maler, L., Longtin, A., Bastian, J., 2003. Non-classical receptive field mediates switch in a sensory neuron's frequency tuning. Nature 423, 77–81.

Chance, F.S., Abbott, L.F., Reyes, A.D., 2002. Gain modulation from background synaptic input. Neuron 35, 773–782.

Colbert, C.M., Magee, J.C., Hoffman, D.A., Johnston, D., 1997. Slow recovery from inactivation of Na^+ channels underlies the activity-dependent attenuation of dendritic action potentials in hippocampal CA1 pyramidal neurons. J. Neurosci. 17, 6512–6521.

Deng, Q., Rashid, A.J., Fernandez, F.R., Turner, R.W., Maler, L., Dunn, R.J., 2005. A C-terminal domain directs Kv3.3 channels to dendrites. J. Neurosci. 25, 11531–11541.

Doiron, B., Chacron, M.J., Maler, L., Longtin, A., Bastian, J., 2003. Inhibitory feedback required for network oscillatory responses to communication but not prey stimuli. Nature 421, 539–543.

Doiron, B., Laing, C., Longtin, A., Maler, L., 2002. Ghostbursting: a novel neuronal burst mechanism. J. Comput. Neurosci. 12, 5–25.

Doiron, B., Lindner, B., Longtin, A., Maler, L., Bastian, J., 2004. Oscillatory activity in electrosensory neurons increases with the spatial correlation of the stochastic input stimulus. Phys. Rev. Lett. 93, 048101.

Doiron, B., Longtin, A., Berman, N., Maler, L., 2001a. Subtractive and divisive inhibition: effect of voltage-dependent inhibitory conductances and noise. Neural Comput. 13, 227–248.

Doiron, B., Longtin, A., Turner, R.W., Maler, L., 2001b. Model of gamma frequency burst discharge generated by conditional backpropagation. J. Neurophysiol. 86, 1523–1545.

Doiron, B., Oswald, A.M., Maler, L., 2007. Interval coding. II. Dendrite-dependent mechanisms. J. Neurophysiol. 97, 2744–2757.

Eggermont, J.J., 1998. Is there a neural code? Neurosci. Biobehav. Rev. 22, 355–370.

Eggermont, J.J., Smith, G.M., 1996. Burst-firing sharpens frequency-tuning in primary auditory cortex. Neuroreport 7, 753–757.

Ermentrout, B., 1996. Type I membranes, phase resetting curves, and synchrony. Neural Comput.. 8, 979–1001.

Fernandez, F.R., Mehaffey, W.H., Molineux, M.L., Turner, R.W., 2005a. High-threshold K^+ current increases gain by offsetting a frequency-dependent increase in low-threshold K^+ current. J. Neurosci. 25, 363–371.

Fernandez, F.R., Mehaffey, W.H., Turner, R.W., 2005b. Dendritic Na^+ current inactivation can increase cell excitability by delaying a somatic depolarizing afterpotential. J. Neurophysiol. 94, 3836–3848.

Fernandez, F.R., Morales, E., Rashid, A.J., Dunn, R.J., Turner, R.W., 2003. Inactivation of Kv3.3 potassium channels in heterologous expression systems. J. Biol. Chem. 278, 40890–40898.

Fleidervish, I.A., Friedman, A., Gutnick, M.J., 1996. Slow inactivation of Na^+ current and slow cumulative spike adaptation in mouse and guinea-pig neocortical neurones in slices. J. Physiol. 493 (Pt 1), 83–97.

Froemke, R.C., Poo, M.M., Dan, Y., 2005. Spike-timing-dependent synaptic plasticity depends on dendritic location. Nature 434, 221–225.

Gabbiani, F., Metzner, W., Wessel, R., Koch, C., 1996. From stimulus encoding to feature extraction in weakly electric fish. Nature 384, 564–567.

Gomez, L., Kanneworff, M., Budelli, R., Grant, K., 2005. Dendritic spike back propagation in the electrosensory lobe of Gnathonemus petersii. J. Exp. Biol. 208, 141–155.

Hansel, D., Mato, G., Meunier, C., 1995. Synchrony in excitatory neural networks. Neural Comput. 7, 307–337.

Hansel, D., Mato, G., Munsiel, C., 1993. Phase reduction in neural modelling. Concepts in Neurosci., 192–210.

Izhikevich, E.M., Desai, N.S., Walcott, E.C., Hoppensteadt, F.C., 2003. Bursts as a unit of neural information: selective communication via resonance. Trends Neurosci.. 26, 161–167.

Jung, H.Y., Mickus, T., Spruston, N., 1997. Prolonged sodium channel inactivation contributes to dendritic action potential attenuation in hippocampal pyramidal neurons. J. Neurosci. 17, 6639–6646.

Kepecs, A., Lisman, J., 2003. Information encoding and computation with spikes and bursts. Network 14, 103–118.

Kepecs, A., Wang, X.J., Lisman, J., 2002. Bursting neurons signal input slope. J. Neurosci. 22, 9053–9062.

Krahe, R., Gabbiani, F., 2004. Burst firing in sensory systems. Nat. Rev. Neurosci. 5, 13–23.

Laing, C.R., Doiron, B., Longtin, A., Noonan, L., Turner, R.W., Maler, L., 2003. Type I burst excitability. J. Comput. Neurosci. 14, 329–342.

Laing, C.R., Longtin, A., 2002. A two-variable model of somatic-dendritic interactions in a bursting neuron. Bull. Math. Biol. 64, 829–860.

Larkum, M.E., Rioult, M.G., Luscher, H.R., 1996. Propagation of action potentials in the dendrites of neurons from rat spinal cord slice cultures. J. Neurophysiol. 75, 154–170.

Lemon, N., Turner, R.W., 2000. Conditional spike backpropagation generates burst discharge in a sensory neuron. J. Neurophysiol. 84, 1519–1530.

Lesica, N.A., Stanley, G.B., 2004. Encoding of natural scene movies by tonic and burst spikes in the lateral geniculate nucleus. J. Neurosci. 24, 10731–10740.

Lesica, N.A., Weng, C., Jin, J., Yeh, C.I., Alonso, J.M., Stanley, G.B., 2006. Dynamic encoding of natural luminance sequences by LGN bursts. PLoS Biol. 4, e209.

Lewis, J.E., Maler, L., 2002. Dynamics of electrosensory feedback: short-term plasticity and inhibition in a parallel fiber pathway. J. Neurophysiol. 88, 1695–1706.

Lewis, J.E., Maler, L., 2004. Synaptic dynamics on different time scales in a parallel fiber feedback pathway of the weakly electric fish. J. Neurophysiol. 91, 1064–1070.

Lindner, B., Doiron, B., Longtin, A., 2005. Theory of oscillatory firing induced by spatially correlated noise and delayed inhibitory feedback. Phys. Rev. E Stat. Nonlin. Soft. Matter. Phys. 72, 061919.

Lisman, J.E., 1997. Bursts as a unit of neural information: making unreliable synapses reliable. Trends Neurosci. 20, 38–43.

Longtin, A., Doiron, B., Bulsara, A.R., 2002. Noise-induced divisive gain control in neuron models. Biosystems 67, 147–156.

Ma, M., Koester, J., 1995. Consequences and mechanisms of spike broadening of R20 cells in Aplysia californica. J. Neurosci. 15, 6720–6734.

Ma, M., Koester, J., 1996. The role of K^+ currents in frequency-dependent spike broadening in Aplysia R20 neurons: a dynamic-clamp analysis. J. Neurosci. 16, 4089–4101.

MacIver, M.A., Sharabash, N.M., Nelson, M.E., 2001. Prey-capture behavior in gymnotid electric fish: motion analysis and effects of water conductivity. J. Exp. Biol. 204, 543–557.

Magee, J.C., Carruth, M., 1999. Dendritic voltage-gated ion channels regulate the action potential firing mode of hippocampal CA1 pyramidal neurons. J. Neurophysiol. 82, 1895–1901.

Maler, L., 1979. The posterior lateral line lobe of certain gymnotoid fish: quantitative light microscopy. J. Comput. Neurol. 183, 323–363.

Maler, L., Mugnaini, E., 1994. Correlating gamma-aminobutyric acidergic circuits and sensory function in the electrosensory lateral line lobe of a gymnotiform fish. J. Comput. Neurol. 345, 224–252.

Maler, L., Sas, E.K., Rogers, J., 1981. The cytology of the posterior lateral line lobe of high-frequency weakly electric fish (Gymnotidae): dendritic differentiation and synaptic specificity in a simple cortex. J. Comput. Neurol. 195, 87–139.

Marsat, G., Pollack, G.S., 2006. A behavioral role for feature detection by sensory bursts. J. Neurosci. 26, 10542–10547.

Mehaffey, W.H., Doiron, B., Maler, L., Turner, R.W., 2005. Deterministic multiplicative gain control with active dendrites. J. Neurosci. 25, 9968–9977.

Mehaffey, W.H., Fernandez, F.R., Maler, L., Turner, R.W., 2007. Regulation of burst dynamics improves differential encoding of stimulus frequency by spike train segregation. J. Neurophysiol. 98, 939–951.

Mehaffey, W.H., Fernandez, F.R., Rashid, A.J., Dunn, R.J., Turner, R.W., 2006. Distribution and function of potassium channels in the electrosensory lateral line lobe of weakly electric apteronotid fish. J. Comput. Physiol. A Neuroethol. Sens. Neural. Behav. Physiol. 192, 637–648.

Mehaffey, W.H., Maler, L., Turner, R.W., 2008. Intrinsic frequency tuning in ELL pyramidal cells varies across electrosensory maps. J. Neurophysiol. 99, 2641–2655.

Metzner, W., Juranek, J., 1997. A sensory brain map for each behavior? Proc. Natl. Acad. Sci. USA 94, 14798–14803.

Metzner, W., Koch, C., Wessel, R., Gabbiani, F., 1998. Feature extraction by burst-like spike patterns in multiple sensory maps. J. Neurosci. 18, 2283–2300.

Middleton, J.W., Longtin, A., Benda, J., Maler, L., 2006. The cellular basis for parallel neural transmission of a high-frequency stimulus and its low-frequency envelope. Proc. Natl. Acad. Sci. USA 103, 14596–14601.

Mitchell, S.J., Silver, R.A., 2003. Shunting inhibition modulates neuronal gain during synaptic excitation. Neuron 38, 433–445.

Murphy, B.K., Miller, K.D., 2003. Multiplicative gain changes are induced by excitation or inhibition alone. J. Neurosci. 23, 10040–10051.

Noonan, L., Doiron, B., Laing, C., Longtin, A., Turner, R.W., 2003. A dynamic dendritic refractory period regulates burst discharge in the electrosensory lobe of weakly electric fish. J. Neurosci. 23, 1524–1534.

Oswald, A.M., Chacron, M.J., Doiron, B., Bastian, J., Maler, L., 2004. Parallel processing of sensory input by bursts and isolated spikes. J. Neurosci. 24, 4351–4362.

Oswald, A.M., Doiron, B., Maler, L., 2007. Interval coding. I. Burst interspike intervals as indicators of stimulus intensity. J. Neurophysiol. 97, 2731–2743.

Prescott, S.A., De Koninck, Y., 2003. Gain control of firing rate by shunting inhibition: roles of synaptic noise and dendritic saturation. Proc. Natl. Acad. Sci. USA 100, 2076–2081.

Rashid, A.J., Dunn, R.J., Turner, R.W., 2001a. A prominent soma-dendritic distribution of Kv3.3 K^+ channels in electrosensory and cerebellar neurons. J. Comput. Neurol. 441, 234–247.

Rashid, A.J., Morales, E., Turner, R.W., Dunn, R.J., 2001b. The contribution of dendritic Kv3 K^+ channels to burst threshold in a sensory neuron. J. Neurosci. 21, 125–135.

Reyes, A., 2001. Influence of dendritic conductances on the input-output properties of neurons. Annu. Rev. Neurosci. 24, 653–675.

Reyes, A.D., Fetz, E.E., 1993. Effects of transient depolarizing potentials on the firing rate of cat neocortical neurons. J. Neurophysiol. 69, 1673–1683.

Rieke, F., 1997. Spikes: Exploring the Neural Code. MIT Press, Cambridge, Mass.

Rinzel, J., 1985. Excitation dynamics: insights from simplified membrane models. Fed. Proc. 44, 2944–2946.

Rinzel, J., Ermentrout, B., 1998. Analysis of neural excitability and oscillations. In: Koch, C., Segev, I. (Eds.), Methods in Neuronal Modelling: From Synapses to Networks. MIT Press.

Salinas, E., Sejnowski, T.J., 2000. Impact of correlated synaptic input on output firing rate and variability in simple neuronal models. J. Neurosci. 20, 6193–6209.

Sawtell, N.B., Williams, A., Bell, C.C., 2007. Central control of dendritic spikes shapes the responses of Purkinje-like cells through spike timing-dependent synaptic plasticity. J. Neurosci. 27, 1552–1565.

Shao, L.R., Halvorsrud, R., Borg-Graham, L., Storm, J.F., 1999. The role of BK-type Ca2+-dependent K^+ channels in spike broadening during repetitive firing in rat hippocampal pyramidal cells. J. Physiol. 521 (Pt 1), 135–146.

Sjostrom, P.J., Hausser, M., 2006. A cooperative switch determines the sign of synaptic plasticity in distal dendrites of neocortical pyramidal neurons. Neuron 51, 227–238.

Smith, G.T., Unguez, G.A., Weber, C.M., 2006. Distribution of Kv1-like potassium channels in the electromotor and electrosensory systems of the weakly electric fish *Apteronotus leptorhynchus*. J. Neurobiol. 66, 1011–1031.

Soltesz, I., 2006. Diversity in the Neuronal Machine: Order and Variability in Interneuronal Microcircuits. Oxford University Press, Oxford, NY.

Stuart, G., Hausser, M., 1994. Initiation and spread of sodium action potentials in cerebellar Purkinje cells. Neuron 13, 703–712.

Tiesinga, P.H., Jose, J.V., Sejnowski, T.J., 2000. Comparison of current-driven and conductance-driven neocortical model neurons with Hodgkin-Huxley voltage-gated channels. Phys. Rev. E Stat. Phys. Plasmas Fluids Relat. Interdiscip. Topics 62, 8413–8419.

Turner, R.W., Lemon, N., Doiron, B., Rashid, A.J., Morales, E., Longtin, A., Maler, L., Dunn, R.J., 2002. Oscillatory burst discharge generated through conditional backpropagation of dendritic spikes. J. Physiol. Paris 96, 517–530.

Turner, R.W., Maler, L., Deerinck, T., Levinson, S.R., Ellisman, M.H., 1994. TTX-sensitive dendritic sodium channels underlie oscillatory discharge in a vertebrate sensory neuron. J. Neurosci. 14, 6453–6471.

Turner, R.W., Meyers, D.E., Richardson, T.L., Barker, J.L., 1991. The site for initiation of action potential discharge over the somatodendritic axis of rat hippocampal CA1 pyramidal neurons. J. Neurosci. 11, 2270–2280.

Ulrich, D., 2003. Differential arithmetic of shunting inhibition for voltage and spike rate in neocortical pyramidal cells. Eur. J. Neurosci. 18, 2159–2165.

Van Goor, F., LeBeau, A.P., Krsmanovic, L.Z., Sherman, A., Catt, K.J., Stojilkovic, S.S., 2000. Amplitude-dependent spike-broadening and enhanced Ca(2+) signaling in GnRH-secreting neurons. Biophys. J. 79, 1310–1323.

Vu, E.T., Krasne, F.B., 1992. Evidence for a computational distinction between proximal and distal neuronal inhibition. Science 255, 1710–1712.

Wang, W., Jones, H.E., Andolina, I.M., Salt, T.E., Sillito, A.M., 2006. Functional alignment of feedback effects from visual cortex to thalamus. Nat. Neurosci. 9, 1330–1336.

Zupanc, G.K., Sirbulescu, R.F., Nichols, A., Ilies, I., 2006. Electric interactions through chirping behavior in the weakly electric fish, *Apteronotus leptorhynchus*. J. Comput. Physiol. A Neuroethol. Sens. Neural. Behav. Physiol. 192, 159–173.